CAMERA CALIBRATION BY AN INTEGRATING SPHERE FOR THE AURORAL TOMOGRAPHY OBSERVATION

Akira Urashima[1], Takehiko Aso[2], Masaki Ejiri[2],
Åke Steen[3], U. Brändström[3] and B. Gustavsson[3]

[1] Department of Electrical Engineering, Kyoto University, Sakyo-ku, Kyoto 606-8501
[2] National Institute of Polar Research, Kaga 1-chome, Itabshi-ku, Tokyo 173-8515
[3] Swedish Institute of Space Physics, Sweden

Abstract: Auroral tomography is a technique to reconstruct three-dimensional (3 D) luminous structure from multiple two-dimensional (2D) images of aurora. The reconstructed auroral luminous structure can provide useful information such as altitude profiles and vortex configuration. In order to obtain the absolute volume emission rate of the aurora distribution, it is essential to have the absolute sensitivity calibration of imaging by formulating the relation between pixel values and absolute brightness of corresponding direction of each pixel. The relation between pixel value and brightness is formulated and calculated from the absolute sensitivity calibration. We took the flat-field images of the integrating sphere calibration standard at National Institute of Polar Research using one camera system, which was installed at Merasjärvi (one of the ALIS observing site, ALIS is the acronym of Auroral Large Imaging System, which is a multi-station ground-based optical observing network). National Institute of Polar Research, Japan and Swedish Institute of Space Physics in Kiruna, Sweden have carried out collaborative observations for auroral tomography under ALIS. The sensitivity calibration result is applied to the reconstruction of volume emission rate distribution from the tomographic images observed by ALIS on March 1, 1998.

1. Introduction

Auroral images are the projection of auroral luminous structure, along the line of sight onto a 2D plane (*e.g.* on the CCD pixels of the camera). A tomographic technique has been applied to reconstruct spatial luminosity distribution from simultaneous multiple images obtained by ALIS. The ALIS is a multi-station optical imaging network at northern Sweden, where collaborative observations for auroral tomography have been carried out by National Institute of Polar Research and Swedish Institute of Space Physics since 1995 using ALIS (Steen *et al.*, 1990, 1997; Aso *et al.*, 1998). In order to apply tomographic technique, it is necessary to obtain the relative sensitivity of each camera image and of each pixel in the same image. For inter-camera sensitivity calibration, we have used the images of the phosphor standard light source, and for inter-pixel sensitivity, we have used the vignetting characteristics. The phosphor sensitivity calibration is a little rough method and in some cases the calculated inter-pixel sensitivity does not reproduce the actual excessive vignetting. Hence, the relative

sensitivity of images and pixels are adjusted so as to minimize the difference between sensitivity adjusted images and corresponding projected images from the reconstructed 3D luminous structure.   Until now, we used the adjusted relative sensitivity calibration for auroral tomography and obtained non-absolute reconstructed results.   However, even if the absolute sensitivity of each pixel and flat field characteristic are to be measured for one camera, we can reconstruct absolute volume emission rate of aurora by incorporating the adjusted relative sensitivity.

2.   Absolute Sensitivity Calibration Method

While the sensitivity calibration with phosphor gives a relative calibration between cameras, the method described here enables us to obtain the absolute radiance value of aurora emission incident on the camera.   The camera system to be calibrated is one of the ALIS cameras, a cooled monochromatic CCD camera with interference filters at wavelengths of 427.8 nm, 557.7 nm, 630.0 nm and 844.6 nm.   The field-of-view is about 85° while it was 54° for all other cameras.   A half power width of the filters is about 4 nm.   The CCD imager, whose size is 1024×1024, uses quad outputs and quad 16 bit A/D converters to increase the readout frequency while maintaining a low readout noise.   By binning neighboring CCD cells on the imager, the sensitivity is increased though the spatial resolution is reduced.   An object at infinity is focused on the CCD plane through a filtered telecentric lens with maximum ray angle of 7°.   We assume that the object stands still during the exposure time, and that A/D converter is linear and does not saturate.   A gray level g_i for a pixel i is expressed by the spectral radiant flux $\Phi_i(\lambda)$ on the corresponding CCD cell as follows:

$$g_i = \left[(A_i \int \eta(\lambda) \Phi_i(\lambda) d\lambda \cdot (t + B_i) + C_i \cdot t + D_i \right], \tag{1}$$

λ: wavelength [nm], $\eta(\lambda)$: CCD quantum efficiency [C/photons],

t: exposure time [s], $[\cdot]$: Gauss function,

A_i: sensitivity of pixel i [counts/C],

B_i: deviation of exposure time [s],

C_i: dark current output of pixel i [counts/s],

D_i: bias of A/D converter of pixel i [counts].

Let $l(x, y, \phi, \theta, \lambda)$ represent the spectral radiance at the position (x, y) on the lens surface in the direction (ϕ, θ).   The spectral radiant flux Φ_i of pixel i comes from the column-like region through the lens system (front lens, telecentric lens and interference filter) as shown in Fig. 1 with:

$$\Phi_i(\lambda) = \int_{\Omega_i} \int_S \eta'(\theta, \lambda) \xi(x, y, \phi, \theta) l(x, y, \phi, \theta, \lambda) \cos \theta \, dS \, d\Omega, \tag{2}$$

where Ω_i is the solid angle of a pixel i, S the area of the lens surface, $\eta'(\theta, \lambda)$ the filter transmittance, and $\xi(x, y, \phi, \theta)$ the transmittance of lens system without the filter to take the vignetting into account.   The filter transmittance characteristic shifts lower in
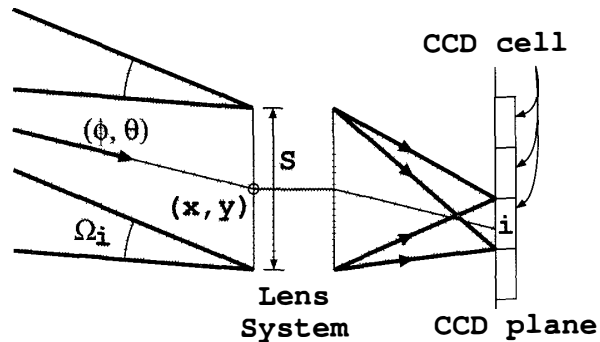
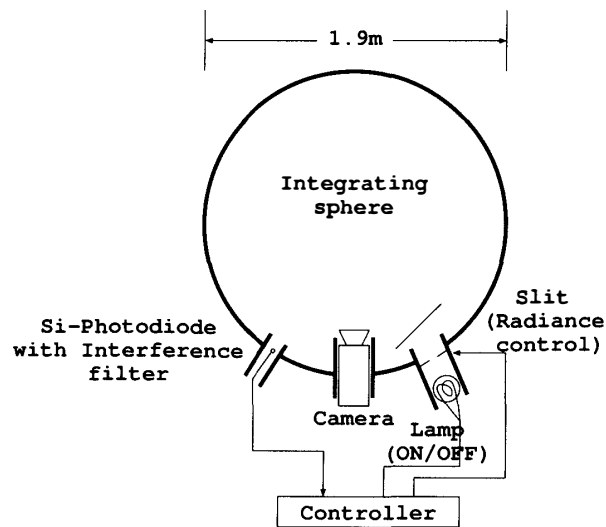Fig. 1.   Optical path to the cell i from column-like region.

Fig. 2.   The integrating sphere calibration standard (OL 462).

wavelengths by some 1 nm for oblique incidence.   As the filter characteristic is rather wide and flat, and also the retrieved aurora shows up in the central part of the image, we assume for simplicity that the filter transmittance for monochromatic aurora dose not differ with the angle of incidence.   More accurate calibration using monochromatic light source is to be conducted.

An integrating sphere calibration standard (OL462) has been installed at National Institute of Polar Research to calibrate absolute sensitivity of optical instruments used for atmospheric probing (OKANO et al., 1998).   It is of a large area and uniform radiant source by injecting coordinated light into the sphere with a perfect diffusing inner surface.   It consists of an integrating sphere, controller, light source and monitoring sensor (as shown in Fig. 2).   The integrating sphere is 1.9 m in its inner diameter, and has 3 windows for a light source, a monitoring sensor and a camera to be calibrated. The radiance uniformity is $\pm 1\%$ for π steradian and $\pm 5\%$ for 2π steradian.   The controller contains the lamp power supply and the display console, and is connected to the the light source and the monitoring sensor.   The light source is a 150 W halogen tungsten lamp with an iris (slit) which adjusts the radiance inside the sphere according to the value on the display console of the controller and the monitoring sensor.   The spectral radiance characteristic of the light source is measured in the wavelengths of

300–1000 nm.   The monitoring sensor is a Si-Photodiode with an interference bandpass filter, whose maximum transmittance wavelength and half power width are 630 nm and 30 nm, respectively. Spectral radiance can be changed in the range of 0.4~4 × 10⁷ R/nm (at 630 nm).

In the case of calibration images, we assume that:

- The radiance is uniform everywhere.
- The bandwidth of the filter of a camera is so narrow that the quantum efficiency of CCD has a constant value η_0.
- The depth of image quantization is sufficient to ignore quantization error.

Then, from eqs. (1) and (2) the gray level g'_i of the pixel i can be written as:

$$g'_i = A'_i l_0 \int \eta'(\lambda) l'(\lambda) d\lambda \cdot t$$

$$+ B'_i l_0 \int \eta'(\lambda) l'(\lambda) d\lambda + C_i \cdot t + D_i, \qquad (3)$$

where

$$A'_i = A_i \eta_0 \int_{\Omega_i} \int_S \xi(x, y, \phi, \theta) \cos\theta \, dS \, d\Omega,$$

$$B'_i = A_i B_i \eta_0 \int_{\Omega_i} \int_S \xi(x, y, \phi, \theta) \cos\theta \, dS \, d\Omega,$$

l_0: spectral radiance of the sphere at 630 nm,
$l'(\lambda)$: spectral radiance characteristic,
($l'(630 \text{ nm}) = 1.0$).

On the other hand, in the case of the observed aurora images, we assume that:

- Aurora is at a great distance so that the radiance in the same direction is uniform at any position of the lens surface.
- The column-like region spanned by one pixel is so small that the radiance of aurora does not vary so much in the region concerned.
- The spectral characteristic of aurora is expressed as a delta function of the wavelength λ_0.

Then, the gray level g''_i of the pixel i can be written as:

$$g''_i = A'_i \eta'(\lambda_0) l''_i t + B'_i \eta'(\lambda_0) l''_i + C_i \cdot t + D_i, \qquad (4)$$

where l''_i is the aurora radiance in the center direction of the column-like region spanned by a pixel i.   As the spectral radiance characteristic of the light source of the integrating sphere and the filter spectral transmittance are calibrated, $\eta'(\lambda_0)$ is known and $\int \eta'(\lambda) l'(\lambda) d\lambda$ can be easily calculated. The unknown parameters of eq. (3), that is, A'_i, B'_i, C_i and D_i are computed by the least-mean-square method from the integrating sphere images by changing the exposure time and radiance l_0. Thus, the aurora radiance l''_i can be obtained by calculating eq. (4).

3. Camera Calibration for Auroral Tomography

3.1. Sensitivity characteristics of the CCD camera

Most of auroral images for tomographic reconstruction have 1–5 s of the exposure time and 1000–20000 counts of the gray level dynamic range. So the images for absolute calibration have seven different exposure times from 0 to 10 s and five intensity levels of the spectral radiance from no light to the radiance just below the saturation of A/D converter. Figure 3 is one example of calibrating images. In this flat-field image, the central part is bright with appreciable vignetting toward the limb. From the difference of quad A/D converters, faint gray level difference among them is evident.

We have calibrated the camera for four filters at the wavelengths of 427.8 nm, 557.7 nm, 630.0 nm and 844.6 nm. For example, images of calibration parameters, A'_i, B'_i, C_i and D_i for a 557.7 nm filter are shown in Fig. 4a–d. Figure 4a is sensitivity parameter image, and 4b is the radiance related parameter image and is independent of the exposure time. Their distributions on the image are very similar, and their ratios are roughly uniform, about 45 ms. It indicates that the exposure time has some deviation. Figure 4c is the parameter image related to the dark current. The value of 4c is about 2–5 counts/s, so this can be ignored. Figure 4d is the image of the bias of A/D converter, and the defect pixel of CCD can be also seen on it. Although the parameter values A'_i or B'_i are different from the value for the other filters, both distributions are very similar in its shape. The parameter values C_i or D_i for all filters are almost similar one another.

The errors in the least mean square method are about 10–20 counts in gray level for each filter. They might be caused by inevitable random noise such as thermal noise.
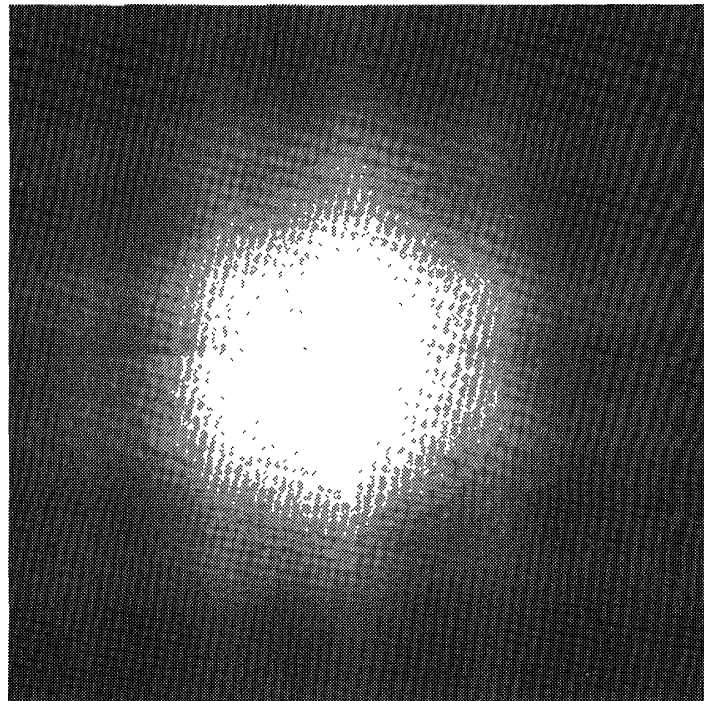

Fig. 3. *The image of the integrating sphere calibration standard (filter: 557.7 nm, exposure time: 10 s, spectral radiance (at 630 nm): 9.853 × 10⁻⁷ W/sr m² nm).*
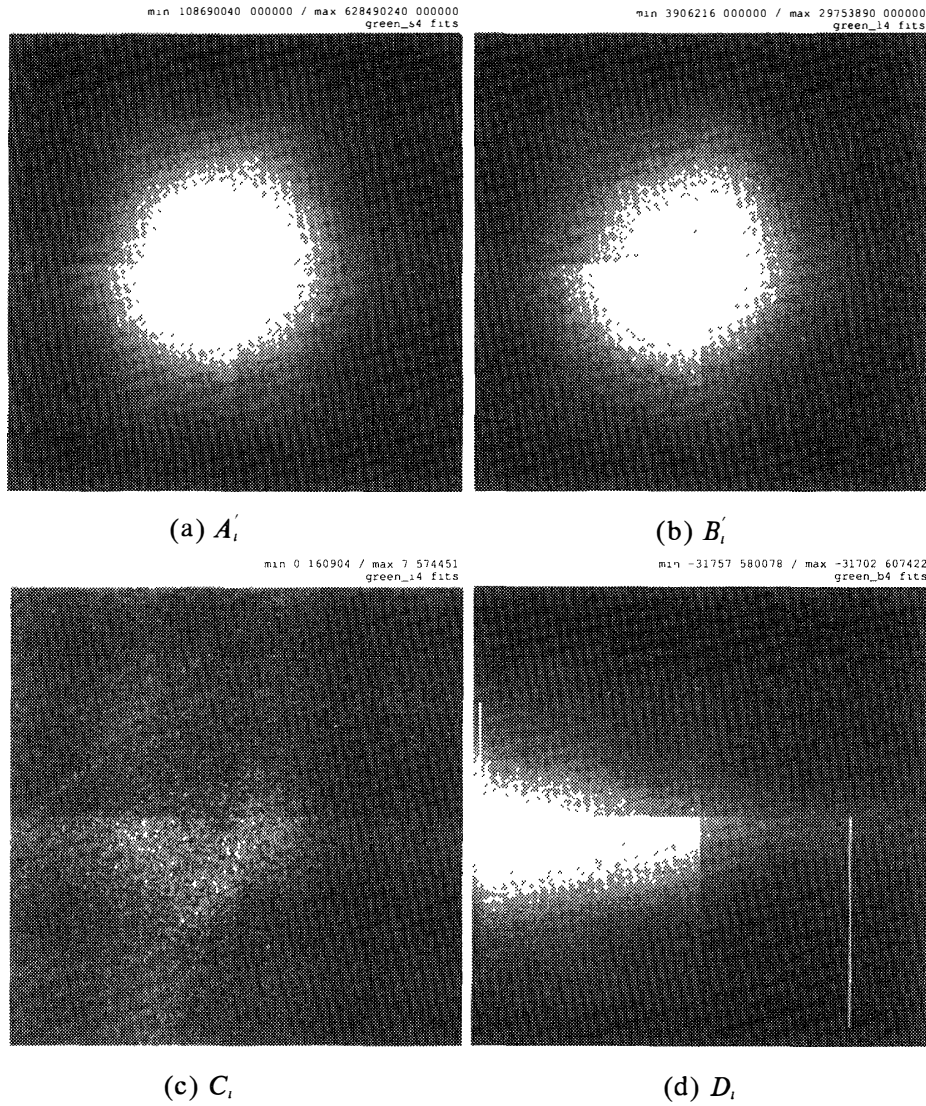
(a) A_i'

(b) B_i'

(c) C_i

(d) D_i

Fig. 4.   The parameter image of the absolute calibration (557.7 nm).

For example, the standard deviation of the difference of two dark images, whose exposure time is 0 s and the radiance of the integrating sphere is zero, is about 13 counts. We can say that the errors are negligible compared to 16 bits dynamic range of the image counts.   The parameter images described here are applied to the absolute sensitivity calibration after removing defective pixels and smoothing to avoid random noise.

3.2. Application to auroral tomography

Aurora emission is assumed to be isotropic.   Also in our applications, aurora arcs are captured in the central part of field-of-view images, so the difference in absorption relative to angle of incidence is not crucial.   Hence, for simplicity, we leave it to future revision to estimate the absorption through the atmosphere.   Then, we express the aurora radiance I_i'' as:

$$I_i'' = \int \frac{L_i(r)r^2 \mathrm{d}r}{4\,\pi r^2} = \frac{1}{4\,\pi} \int L_i(r)\mathrm{d}r, \tag{5}$$

where $L_i(r)$ is the aurora emission rate along the line-of-sight of a pixel i and r is the distance from the camera.   We employ the voxels (volume elements) model to represent the reconstructed spatial distribution of aurora emission, so eq. (5) is rewritten as:

$$l_i'' = \frac{1}{4\pi} \sum_j w_{ij} L_j,$$ (6)

where w_{ij} means how the aurora emission L_j of a voxel j contributes to l_i'' and is equal to the traverse length of the line-of-sight of a pixel i on a voxel j.   Our tomographic reconstruction method is a modified version of SIRT (Simultaneous Iterative Reconstruction Technique) (Aso *et al.*, 1998; URASHIMA *et al.*, 1997) as:

$$\widetilde{L}_j^{(k+1)} = \widetilde{L}_j^{(k)} \prod_i \left(\frac{l_i''}{\widetilde{l}_i''^{(k)}} \right)^{\lambda \frac{w_{ij}}{\sum_i w_{ij}}},$$ (7)

where λ is a relaxation parameter (a typical value is 1.0), $\widetilde{L}_j^{(k)}$ is the reconstructed emission rate of a voxel j at the iteration number k, and $\widetilde{l}_i''^{(k)}$ is the reconstructed aurora radiance.   Equation (7) indicates that each voxel value is modified multiplicatively with the averaged weight so as $\widetilde{l}_i''^{(k)}$ to be close to l_i''.   In addition to this, the so-called "fieldalignedness correction in proximity" is assumed for ill-conditioned auroral tomography in order to add a priori information to the reconstruction, in which altitude profiles along the geomagnetic line of force is averaged in its proximity while keeping the integrated value of each profile.   This method is applied to the reconstructed value by SIRT, and then SIRT iteration is resumed.   This sequence is repeated until the residual
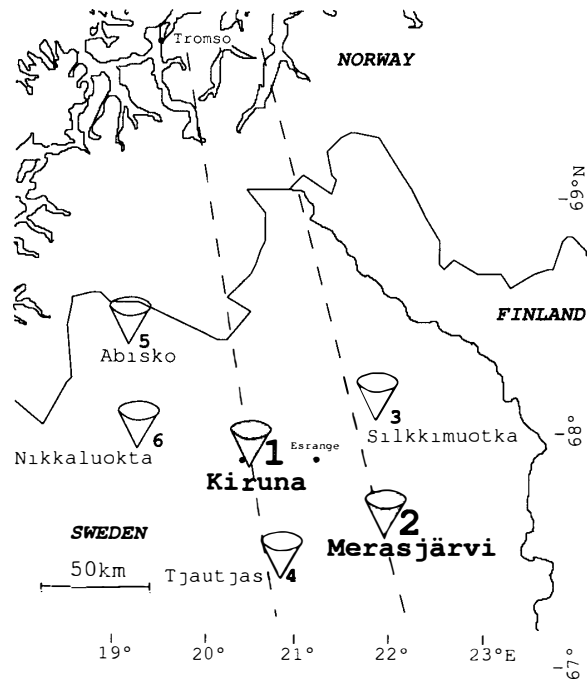

Fig. 5. ALIS observation site map.

of $\tilde{l}_i''^{(k)}$ to l_i'' becomes a minimum.   CT (computed tomography) auroral images of 557.7 nm at 2002:00 UT and of 427.8 nm at 2002:10 UT were obtained at two ALIS sites, Kiruna and Merasjärvi (shown in Fig. 5 by shaded cones) on March 1, 1998. These images are analyzed using SIRT and "field-alignedness correction in proximity". The camera at Merasjärvi is absolutely calibrated, while the camera at Kiruna is not. So the sensitivity of the camera at Kiruna is relatively adjusted to the camera at Merasjärvi.   The images of 557.7 nm and 427.8 nm projected to 100 km height are shown in Fig. 6.

The Visualization of the Reconstructed voxel values are shown in Fig. 7.   The arrow with "N" in the figure indicates geographic north and the wire frame box indicates the voxel region, from 80 km to 220 km in altitude and 90 km in NS and 200 km in EW direction.   The region is divided into voxels of 70(alt.) × 60(NS) × 50(EW). As the brightest aurora arc in the overlap region of the two observed images is selected for the reconstruction, the other part of the image is eliminated in Fig. 7.

Since the reconstructed voxel values are derived from the absolutely calibrated image, the absolute values of the aurora emission can be obtained.   The field-aligned altitude profiles of reconstructed luminosity $\tilde{L}_j$ for the center of the arc of 557.7 nm and
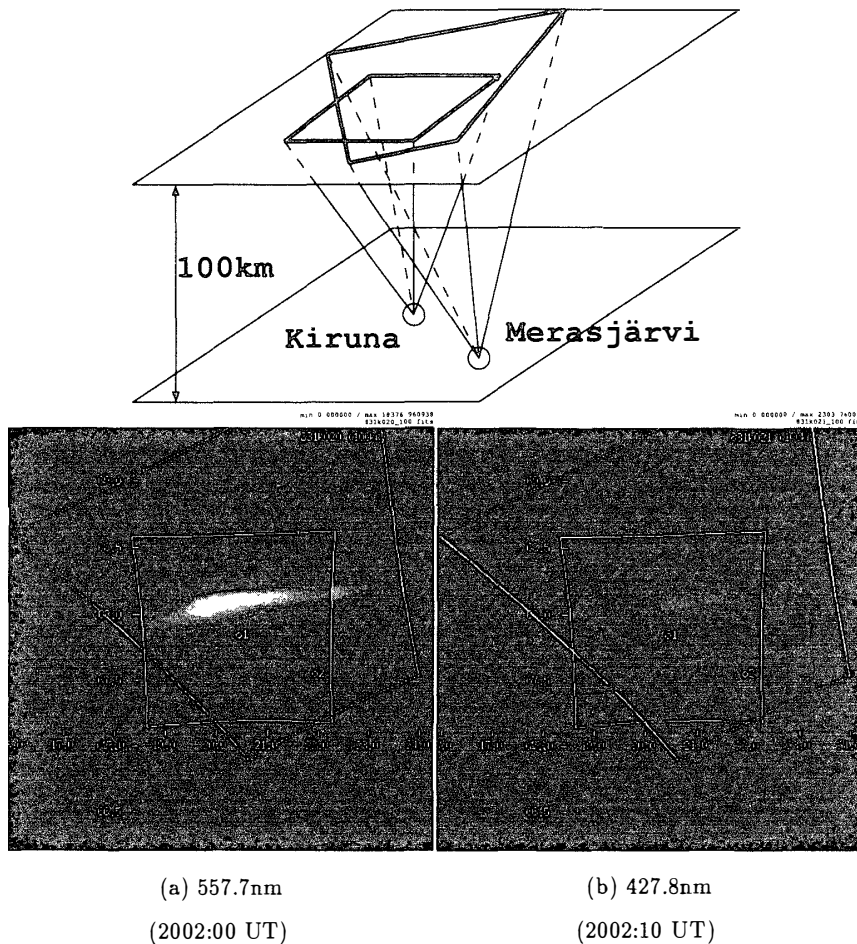

(a) 557.7nm   (b) 427.8nm

(2002:00 UT)   (2002:10 UT)

Fig. 6.   The observed images projected at 100 km height.   The upward direction of the paper is the geographic north.

(a) 557.7nm   (b) 427.8nm
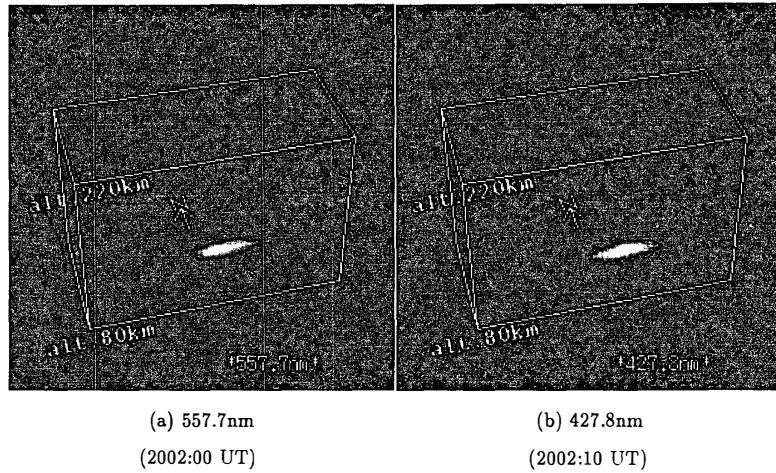
(2002:00 UT)   (2002:10 UT)

Fig. 7.   *Visualization of the reconstructed emission rate.*
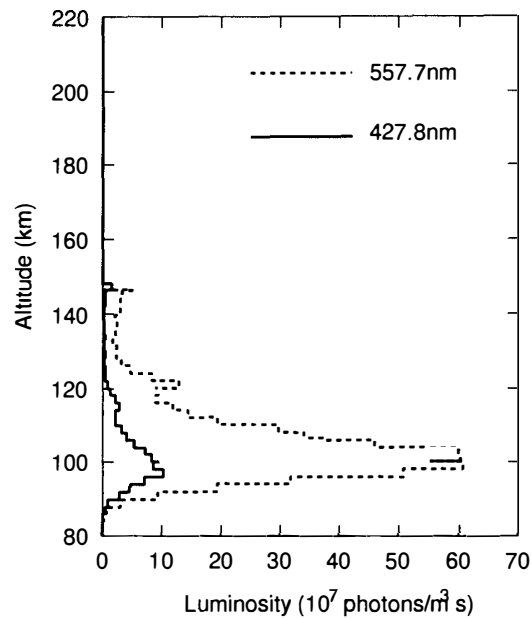

Fig. 8.   *Profiles of the reconstructed emission rate.*

427.8 nm are illustrated in Fig. 8. As the profiles in Fig. 8 are on the same location at almost the same time (only 10 s apart), they can be compared as the spatial distributions of the different wavelengths of the same aurora. The peak value of 557.7 nm is 6.0×10^8 photons/m^{3}s, and about 6–7 times larger than that of 427.8 nm. The peak heights of 557.7 nm and of 427.8 nm are around 100 km. The photoemission rate of 557.7 nm comes from the transition of $O(^1S)$ to $O(^1D)$ and that of 427.8 nm from N_2^+ 1st negative band. Recent theoretical calculation shows that the energization process for direct impact of energetic electon to the oxygen atom produces $O(^1S)$ and gives the maximum volume emission rate at the height around 110 km, while the process for N_2^+ impact gives the maximum emission at 98 km, about 10 km lower than the former (ONDA *et al.*, 1998). However, the present result shows that the peak height for 557.7 nm around 100 km is not significantly different from that for 427.8 nm, which suggests that the

excitation of $O(^1S)$ is closely related to the spatial density of excited nitrogen molecules. That is, the energy transfer process of N_2^+ 1st positive band to $O(^3P)$ may be a dominant process to produce $O(^1S)$. The result of this study also strongly argued that any theory for the above process should also satisfy the condition that the ratio of volume emission rate of 557.7 nm to that of 427.8 nm is around 6–7.

4. Conclusion

The absolute calibration method for auroral tomography is formulated under some simplified assumptions for the monochromatic camera system, the integrating sphere calibration standard and actual auroral imaging. This method is applied to the camera installed at Merasjärvi, one of the ALIS observing site. The calibration results indicate that quad A/D converters do not have the same characteristics and that there are some differences in dark current and deviation of the exposure time. They can be compensated with this absolute calibration results. Although there are some errors in the least-mean-square method to compute the sensitivity parameter etc., the errors are negligible for the aurora images of vast gray level dynamic range. So the absolute calibration results are safely applicable to the auroral CCD camera system. By applying the absolute calibration results, two volume emission rate distributions of the different wavelength were reconstructed from the images observed at Kiruna and Merasjärvi. The ratio of the peak value and the difference of the peak height along the same geomagnetic line of force give some evidence for the production processes of auroral emissions. Although we used only two cameras in this study, it will be possible to obtain more reliable absolute volume emission rate distributions from the ALIS tomography images, after applying our calibration method to all of the camera systems at the observing sites.

References

ASO, T., EJIRI, M., URASHIMA, A., MIYAOKA, H., STEEN, Å., BRÄNDSTROM, U. and GUSTAVSSON, B. (1998): First results of auroral tomography from ALIS-Japan multi-station observation in March, 1995. Earth Planets Space, **50**, 81–86.

OKANO, S., TAKESHITA, S. and TAGUCHI, M. (1998): Absolute calibration system at NIPR for aurora/airglow measurements using a 1.9-m integration sphere. Proc. 24th Annual European Meeting on Atmospheric Studies by Optical Method. Andenes, Norway, 30.

ONDA, K., EJIRI, M., ITIKAWA, Y. and MIYAOKA, H. (1998): Altitude profile of electron density and oxygen green line in active auroral arcs based on electron differential number flux observed by sounding rocket. Proc. NIPR Symp. Upper Atmos. Phys., **11**, 36–54.

STEEN, Å., BRÄNDSTROM, U. and KAILA, K. (1990): A scientific and technical description of ALIS. Proc. NSSR Annual Meeting, Bolkesjö, Norway, 153.

STEEN, Å., BRANDSTRÖM, U., GUSTAVSSON, B. and ASO, T. (1997): ALIS—A multi-station imaging system at high latitude with multi-disciplinary scientific objectives. Proc. 13th ESA symposium on European Rocket and Balloon Programs and related Research, Öland, Sweden. ESA SP-397, 261–266.

URASHIMA, A., FUJITA, T. and ASO, T. (1997): A study of the reconstruction algorithm for auroral tomography by numerical simulation. Nankyoku Shiryô (Antarct. Rec.), **41**, 469–496.